CRANFIELD UNIVERSITY

SAMUEL FRANCESC LOPEZ CANOS

ASSESSMENT OF FATIGUE CRACK PATHS IN SINGLE CRYSTALS FROM TURBINE BLADES

SCHOOL OF AEROSPACE, TRANSPORT AND MANUFACTURING
Aerospace Materials

MSc
Academic Year: 2017–2018

Supervisor: Dr. Gustavo Castelluccio
August 2018

CRANFIELD UNIVERSITY

SCHOOL OF AEROSPACE, TRANSPORT AND MANUFACTURING
Aerospace Materials

MSc

Academic Year: 2017–2018

SAMUEL FRANCESC LOPEZ CANOS

Assessment of Fatigue Crack Paths in Single Crystals from Turbine Blades

Supervisor: Dr. Gustavo Castelluccio
August 2018

This thesis is submitted in partial fulfilment of the requirements for the degree of MSc.

Abstract

Fatigue failures in turbine blades are a pervasive, unresolved economic and safety problem that is leading the structural integrity concern in both Civil and Military Aerospace engines. The high temperatures and the harmful operating environment that blades face in service coupled with the anisotropy of the single crystal nickel-based superalloys converts the fatigue analysis of a turbine blade into an even more intricate matter. As a result, it is necessary to simplify the problem and analyse it under controlled conditions. In an attempt to contribute to the aforementioned, this project explores the change in orientation that fatigue cracks undergo as they grow in notched single crystals. The analysis involves the calculation of the shear stresses resolved on the slip systems as well as the detection of single slip or multislip regions along the crack path. Two models have been created to address the problem: a simplified model without growing the crack and a more complex model growing the crack. Results are provided as i) the evolution of the shear stresses resolved on the slip planes along the crack path (RSS graph) and ii) the fluctuation of Q factor along the crack path (Q factor graph). The simultaneous analysis of both explains the crack path deviations. However, no single slip regions have been found among the specimens analysed due to the low cycle fatigue testing condition. The findings and recommendations of this project may be used to optimise blade design and eventually predict crack path.

Keywords

Single Crystal; Fatigue; Slip systems; Crack path

Contents

List of Figures

List of Tables

List of Abbreviations

CRSS	Critical Resolved Shear Stress
CSYS	Coordinate System
FCC	Face Centered Cubic
FEA	Finite Element Analysis
LCF	Low Cycle Fatigue
LEFM	Linear Elastic Fracture Mechanics
RSS	Resolved Shear Stresses
SATM	School of Aerospace, Technology and Manufacturing

Chapter 1

Introduction

1.1 Background

Fatigue induced failures in turbine blades are a pervasive, unresolved problem that is leading the structural integrity concern in both Civil and Military Aerospace engines.

Current turbine blades are manufactured in single crystals nickel-based superalloys because of their superior creep, stress rupture and thermomechanical fatigue capabilities over polycrystalline alloys [1]. The main feature of these materials is their highly orthotropic properties and heterogeneity. Hence, crystallographic orientation becomes an essential parameter to look at when studying the crack growth behaviour, and new approaches must be tackled to incorporate these effects. In addition, the combination of the corrosive environment, high operating temperatures, high monotonic and cyclic stresses and manufacturing variability add a significant degree of complexity to the fatigue failure mechanism of these structural components, which are expected to live long periods.

Considering all of these aspects, it is essential to approach the problem under controlled conditions and standardised geometries. By doing this, it will be possible to reduce the level of complexity and focus only on the fundamental physics of the failure. Once the problem is understood under simplified conditions, it will be easier to extrapolate those results towards more complex conditions and geometries.

Therefore, gaining knowledge on the fatigue failure mechanisms will help to prevent them and reduce the costs associated to the maintenance and repairs as well as decrease the non-operating times of the affected engines.

1.2 Aim

This project aims to understand the change in orientation that fatigue cracks undergo as they grow in notched single crystals. Figure 1.1[1] depicts this change in orientation for different specimens tested at Cranfield within a program in collaboration with Rolls-Royce. The transition to a slanted orientation has been highlighted in yellow and defined as a departure from the orientation normal to the applied load (in a [001] fatigue test). To approach the solution, the analysis will be focused on investigating the changes in the stress field as cracks advances in single crystals by means of finite element simulations in Abaqus 6.14 software.

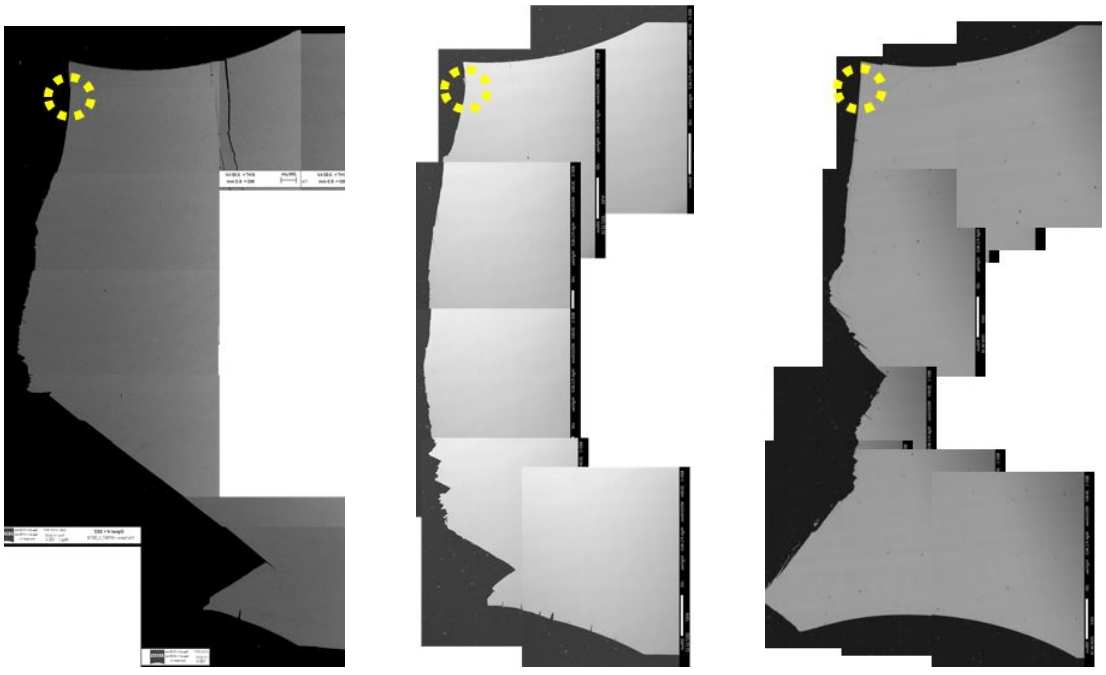

(a) Specimen A (b) Specimen B (c) Specimen C

Figure 1.1: Examples of slanted cracks in single crystal double-notched failed specimens

[1]The cracks are growing from the top to the bottom of the Figure.

The analysis will be restricted to single crystal nickel based superalloys since they are the preferred option for manufacturing turbine blades in a gas turbine engine. Likewise, the geometries and the testing conditions will be limited to the ones already tested within the Rolls-Royce & Cranfield University program. Lastly, the study will be limited to the crack propagation fatigue stage and the only difference between the specimens analysed will be the crystallographic orientation.

1.3 Objectives

The main objectives of the project are:

- Explore the influence that crystallographic orientation and slip systems have in crack growth behaviour.
- Use a three-dimensional elastic anisotropic Finite Element Analysis (FEA) to compute the triaxial stress fields along the crack path.
- Develop a methodology to predict the crack path in the single slip regions.
- Establish a methodology to predict crack deviations in notched single crystals right after the notch intensification dies out.
- Determine if the crack path direction is driven by mechanical propagation.

Chapter 2

Literature Review

Continuous development in manufacturing processes in the last decades has permitted to produce turbine blades as single crystals by using the investment casting technique. This fabrication process allows to obtain a structure with only one grain growing in the preferential direction. The absence of grain boundaries avoid the passages for diffusion and oxidation that grain boundaries provided in polycrystalline materials and eliminates the deformation by grain boundary sliding [2]. Furthermore, the structure becomes anisotropic, generating a strong dependence of the material properties with crystallographic orientation. For turbine blades, the optimum primary orientation (defined by α in Figure 2.1) is the one in which the stacking airfoil line is aligned with the [001] direction. This orientation provides better creep strength and a low modulus of elasticity that improves thermal fatigue resistance [7]. A maximum variation of $\pm 10^{\circ}$ is normally allowed due to manufacturing imprecisions. The secondary orientation (defined by β in Figure 2.1) is the angle formed by the [100] orienation and the airfoil mean chord line. This orientation is randomly oriented, although several studies ([1], [4], [8]) conclude that secondary orientation plays a significant role in crack initiation modes and fatigue life, being capable of increasing the resistance to fatigue crack propagation without adding additional weight or cost. Figure 2.1 depicts the situation of both α and β.

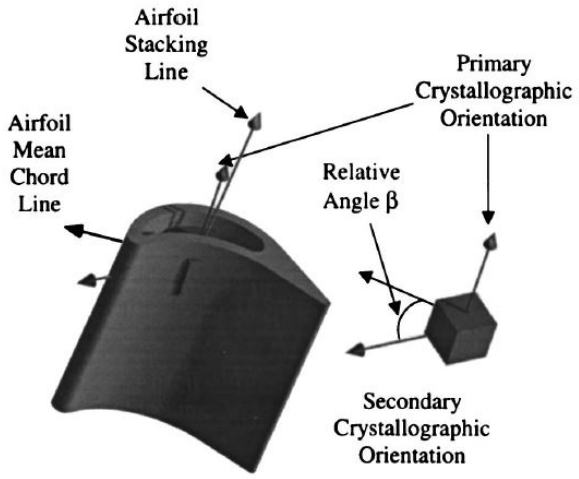

Figure 2.1: Convention for defining crystal orientation in turbine blades [1]

The high temperatures and the harmful operating environment that turbine blades face during service requires a material capable of withstanding this conditions coupled with sufficient strength and processability (i.e. suitability with the investment casting process). With those characteristics, nickel-based superalloys seem to be the most appropiate solution. As mentioned in [9], PWA 1484, René N5 and CMSX-4 are the most widely used single crystal materials for turbine blade applications. The microstructure of these materials consists of a γ matrix (FCC solid solution) with Ni as the primary element and a typically coherent, FCC-like Ni_3Al intermetallic γ' ($L1_2$ crystal structure). Distribution, morphology and volume fraction of γ' are the key factors to control in order to obtain a strong alloy. The different generations of single crystal Ni-based superalloys differ from each other in the volume fraction of γ' precipitates, with the most recent generation reaching levels of 60-70% [9].

As both γ and γ' are FCC structures with similar lattice constants, the whole crystal structure can be considered as an only FCC crystal. Due to this, the structure exhibits cubic symmetry and can be characterised by only three independent elastic constants: Young's modulus (E), shear modulus (G) and Poisson ratio (ν). Therefore, the elastic behaviour of a material exhibiting cubic symmetry can be represented by Hooke's law as

shown in Equation 2.1 (in compliance form) [10].

$$\{\varepsilon\} = \begin{pmatrix} a_{11} & a_{12} & a_{12} & 0 & 0 & 0 \\ a_{12} & a_{11} & a_{12} & 0 & 0 & 0 \\ a_{12} & a_{12} & a_{11} & 0 & 0 & 0 \\ 0 & 0 & 0 & a_{44} & 0 & 0 \\ 0 & 0 & 0 & 0 & a_{44} & 0 \\ 0 & 0 & 0 & 0 & 0 & a_{44} \end{pmatrix} \{\sigma\} \tag{2.1}$$

where:

$$a_{11} = \frac{1}{E} \qquad a_{44} = \frac{1}{G} \qquad a_{12} = -\frac{\nu}{E} \tag{2.2}$$

Equation 2.1 represents the anisotropic elasticity model for a material which exhibits cubic symmetry. Elastic anisotropy can be used under the assumption of small scale yielding, which postulates that if the plastic zone generated at the crack tip is small compared to the rest of the domain (i.e. localised plasticity), the behaviour within this plastic zone will be dominated by the surroundings, which are essentially elastic [11]. This is the principle of the Linear Elastic Fracture Mechanics (LEFM), which is applicable only to the description of long crack kinetics [12]. However, stress intensity range (ΔK), which is the parameter that characterises the crack growth behaviour in LEFM, does not correlate properly in single crystals due to their inherent anisotropy and heterogeneity ([4], [13]). As a consequence, other approaches must be tackled.

The fact of assuming small scale yielding does not exclude completely plastic deformation of the analysis that is being done. As nickel-based superalloys are inherently ductile, plasticity precedes fracture and regions of plastic deformation form in the neighbourhood of the crack tip. Because of that, it is essential to understand how plastic deformation appears and develops during the fatigue mechanism in single crystal alloys. Therefore, it is necessary to introduce the concept of slip system and study the dislocation theory.

As explained in [2], dislocation motion occurs exclusively in preferred crystallographic planes along specific crystallographic directions. Preferred crystallographic planes are the ones with the greatest planar density (i.e. close packed planes) and are normally called slip planes. Preferred crystallographic directions are the directions in the slip plane with the highest linear density (i.e. close packed directions) and are normally called slip directions. The combination of slip plane and slip direction is called slip system. Dislocation motion follows the shortest possible atomic distances so that the material stores minimum energy while deforming [2]. The FCC structure of nickel-based superalloys has 12 slip systems: 4 $\{111\}$ slip planes and 3 $<1\bar{1}0>$ slip directions in each slip plane. The combination of the 4 slip planes along with with their reciprocals forms an octahedral. This is the reason why in some cases they are referred as the octahedral slip systems of the FCC structure. Table 2.1 summarizes these 12 slip systems and Figure 2.2 depicts an example of those.

Slip System	Slip Plane	Slip Direction
1	(1 1 1)	[1 0 $\bar{1}$]
2	(1 1 1)	[0 $\bar{1}$ 1]
3	(1 1 1)	[1 $\bar{1}$ 0]
4	($\bar{1}$ 1 $\bar{1}$)	[1 0 $\bar{1}$]
5	($\bar{1}$ 1 $\bar{1}$)	[1 1 0]
6	($\bar{1}$ 1 $\bar{1}$)	[0 1 1]
7	(1 $\bar{1}$ $\bar{1}$)	[1 1 0]
8	(1 $\bar{1}$ $\bar{1}$)	[0 $\bar{1}$ 1]
9	(1 $\bar{1}$ $\bar{1}$)	[1 0 1]
10	($\bar{1}$ $\bar{1}$ 1)	[0 1 1]
11	($\bar{1}$ $\bar{1}$ 1)	[1 0 1]
12	($\bar{1}$ $\bar{1}$ 1)	[1 $\bar{1}$ 0]

Table 2.1: Slip plane and slip direction for the 12 octahedral slip systems of the FCC structure [4]

Dislocation motion in crystalline materials leads to plastic deformation [2]. This type of linear defects arises in surface irregularities or internal defects which act as stress concentrators during deformation. The motion of these dislocations is uniquely driven by shear stresses and their onset can be predicted by Schmid's Law [7]. The shear stresses

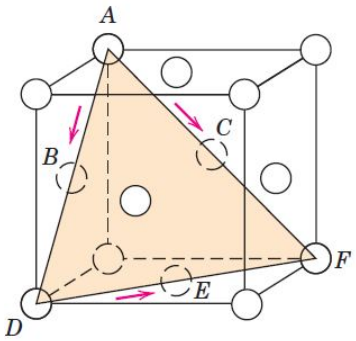

Figure 2.2: Representation of slip systems in a FCC structure [2]

resolved on the slip planes control plastic deformation and, consequently, crack growth behaviour (instead of the maximum principle stress in polycrystalline materials).

Equation 2.3 represents Schmid's Law, which quantifies the shear stresses (τ^{α}) resolved in the slip system α:

$$\tau^{\alpha} = m^{\alpha}\,\sigma\,n^{\alpha} = \frac{F}{A}\cos(\phi^{\alpha})\cos(\lambda^{\alpha}) \tag{2.3}$$

where m^{α} is the slip direction in the slip plane, n^{α} is the normal to the slip plane, ϕ^{α} is the angle between F and the normal to the slip plane and λ^{α} is the angle between F and the slip direction [2].

Equation 2.3 can be used to predict the onset of yield in single crystals. This onset is determined by the Critical Resolved Shear Stress (CRSS), which is a material property independent of the loading direction. According to this, slip will occur on the slip system with the highest resolved shear stress (RSS) as long as the applied load is high enough to reach the CRSS [4]. However, CRSS varies significantly with continuous plastic deformation leading to hardening response by virtue of dislocations interaction [14]. Consequently, it can be used to accurately predict the onset of yield, but it may introduce errors after initiation of plasticity. Furthermore, CRSS is dependent on the temperature, heat treatment condition and volume fraction of γ'. For CMSX-4 at 550°C, CRSS=376 MPa for the octahedral slip systems [6].

The reason why it has been introduced the bases of the dislocations theory is that

crack growth is caused by the cyclic plastic deformation of the crack tip and hence is due to the emission of dislocations from this particular stress intensification [15]. Dislocation emission along slip planes cause the blunting of the crack tip and the appearance of shear bands ahead of it. Re-sharpening and crack tip advancing occurs when the applied stress is reversed [5]. Through this process, the majority of dislocations that are emitted get back to the surface and disappear (reversible process), whilst the residual part remain in the material and contribute to crack growth (irreversible process).

Likewise, fatigue cracks in single crystals usually develop and propagate along well-defined crystallographic slip planes [3] (see Figure 2.3). Consequently, crack path is dependent on the number of slip systems that are emitting dislocations simultaneously. If several slip systems are emitting dislocations, there is a multiple slip condition, and each of these slip systems will be contributing to the crack direction (alternating shear mechanism). By contrast, if there is only one slip system emitting dislocations, there is a single slip condition (i.e. only one slip system is contributing to crack growth). In this condition, the crack path will necessarily follow the direction of this particular plane. Therefore, under single slip conditions, it will be easier to identify and eventually predict the crack path.

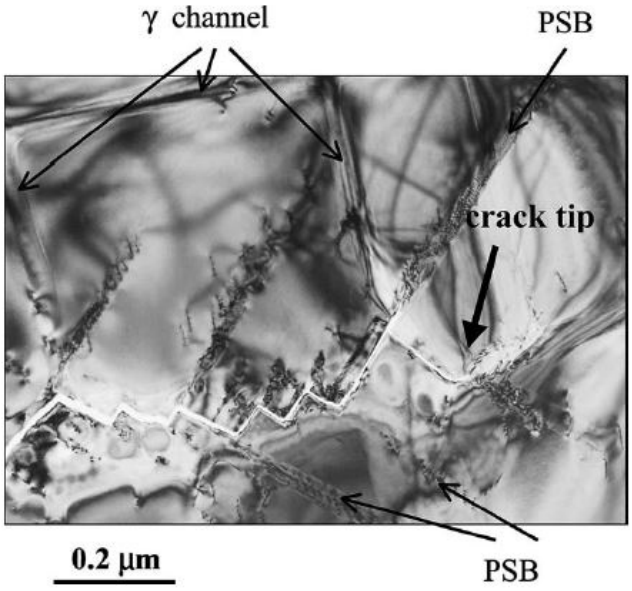

Figure 2.3: Multislip cracking region along $\{111\}$ planes in a CMSX-4 superalloy [3]

In order to differentiate single slip from multiple slip conditions, the authors in [16] introduced a parameter called Q factor, which is defined as the ratio of the Schmid factor of the secondary system to that of the primary. Hence, a Q factor close to 1 indicates a clear tendency to multislip whilst a good single slip condition corresponds to Q less than 0.9 [16]. However, further work [16] made in this area found a single slip condition with a Q factor of 0.933 in single crystal copper alloys. Thus, there is not a well-defined boundary to separate both conditions and the value should range between 0.9 and 0.933. Figure 2.5 depicts an example of a multislip condition, with several distinct slip traces appearing in the neighbourhood of the notch indicating multiple slip systems activation as a result of the stress intensification.

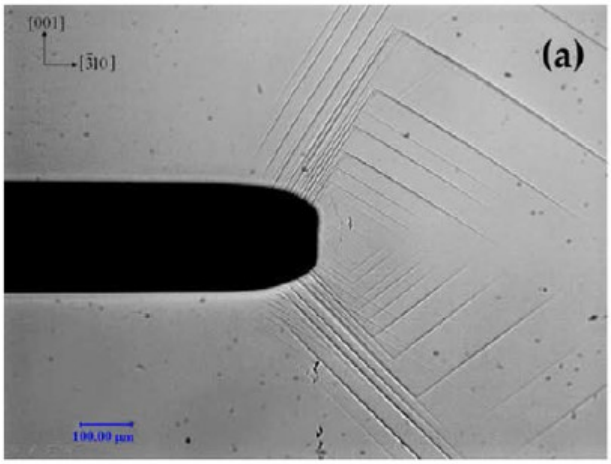

Figure 2.4: Example of multiple slip traces along different planes near the notch [4]

Although $Q = 1$ and $Q = 0.9$ are only one tenth difference, they are indicating contrary slip conditions. This may seem controversial, but there is a reason behind. Figure 2.5 represents a hysteresis loop for a single crystal alloy. As it can be seen, when reaching plasticity conditions, the change in strain is much more significant than the change in stress. As the Q factor is based on stress, the difference between the shear stresses that promote plasticity is not as notable as if the Q factor was based on strain. That is the reason why only one tenth difference implies different slip conditions.

Ultimately, crack growth rate differs substantially if the crack is growing along single slip conditions rather than in multiple slip conditions. Experimental results in [17]

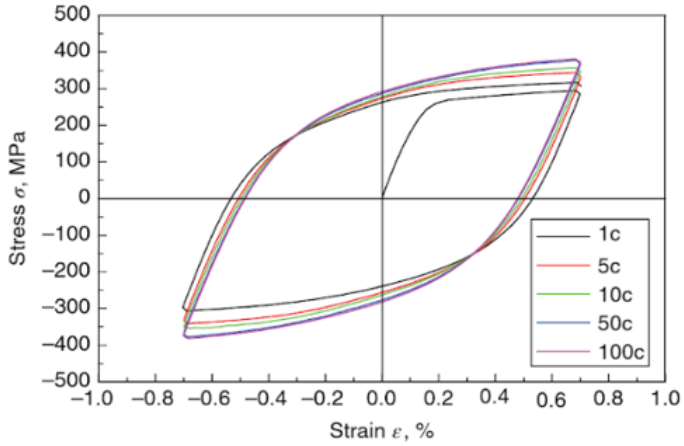

Figure 2.5: Hysteresis loop from a single crystal alloy [5]

demonstrated that the failure mode affects the fatigue crack growth rate. In their study, it was found that a crack propagating along two competing slip systems (i.e. multislip condition) along a plane perpendicular to the applied load grows faster than a crack growing in a single slip condition along the preferred slip plane. This statement may be used to optimise the design of the blades by selecting the orientation that contributes to grow the crack under single slip conditions for a specific loading condition.

Chapter 3

Methodology

3.1 Introduction

This chapter explains the methodology followed to understand and eventually predict the crack path in notched single crystals. This procedure is intended to be an automated, replicating process created with the aim of estimating: i) when the crack is going to departure from the normal direction and ii) what direction is going to take (see Figure 1.1 for further clarification). The analysis will be based on an anisotropic elastic model under the assumption of small scale yielding. The material used in the simulations will be the actual one used by Rolls-Royce in their engines: CMSX-4.

A brief summary of the methodology is depicted in Figure 3.1. This simplified flowchart starts with the inputs required to develop the analysis, followed by the pre-processing (e.g. material properties definition) and the post-processing (e.g. stress state output) parts of the FEA. The two main software that are going to be used are Abaqus as the Finite Element code and Matlab as the post-processing tool.

As mentioned in Chapter 2, the shear stresses resolved on the slip systems are controlling plastic deformation and crack growth behaviour. The procedure explained here gathers how to quantify them as well as other aspects related to the development of the FE model used to approach the solution.

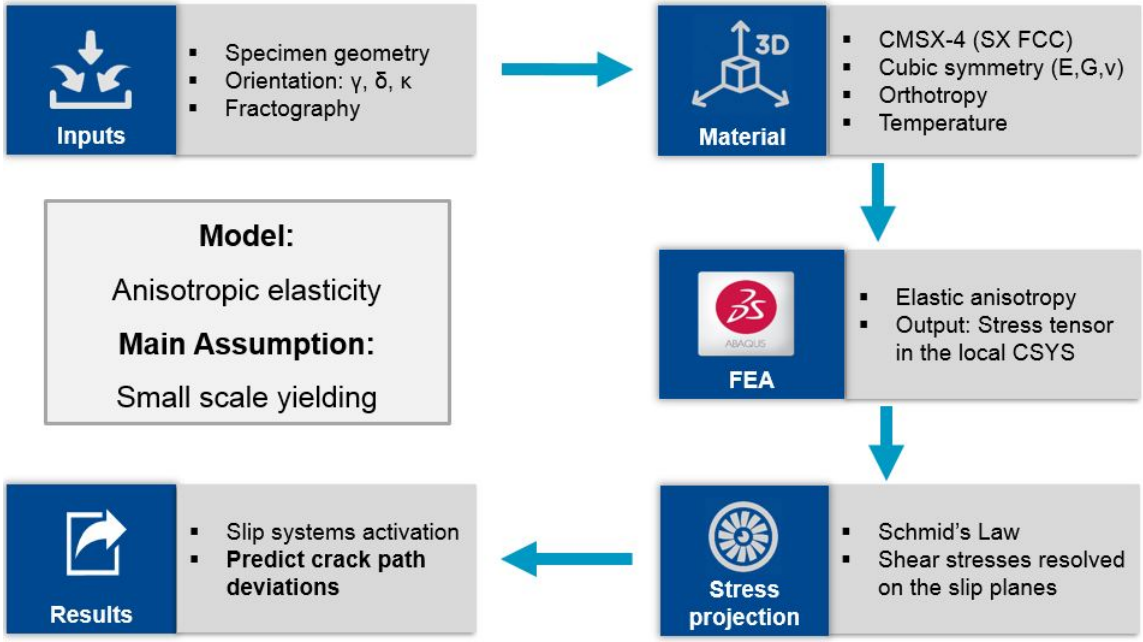

Figure 3.1: Brief summary of the methodology

3.2 Geometry and testing conditions

The complex geometry and operational conditions that blades face during service makes the fatigue problem an intricate challenge to address under these circumstances. As a result, it is necessary to approach the problem under controlled conditions and simplified geometries. Both of them have been previously defined by the Rolls-Royce and Cranfield University program. This work will be limited to use the experimental results obtained in this program and try to explain the crack behaviour by means of FE simulations looking at the fractography images. Table 3.1 gathers the testing conditions. Figure 3.2 shows the geometry of the samples. Appendix A gathers the detailed measures of the simulated sample.

A key point to consider is that the specimens were tested under a mixture of air and sulphur dioxide (SO_2). The role of sulphur as well as other corrosion products in the crack propagation stage is a question underlying the project[1]. The simulations described here are performed as if the samples were tested in a corrosion-free environment. If the crack

[1]It is assumed that the corrosion and oxidation products play a significant role in the incubation and initiation of the crack, but there is no evidence about the role in the propagation of the crack.

path can be explained in these conditions, the crack propagation stage will be driven only by mechanics. By contrast, if the results do not match the experimental ones, corrosion and oxidation may be playing a role in the propagation of the crack. Ultimately, the samples were tested in the low cyclic fatigue (LCF) regime.

Condition	Value
Material	CMSX-4
Temperature	550°C
Nominal Stress (at notch base)	419 MPa
Notch	$k_t = 1.38$
Salt Load	0.6 mg/cm^2
SO_x	50 ppm
Cycle type	1_1_1_1

Table 3.1: Testing conditions

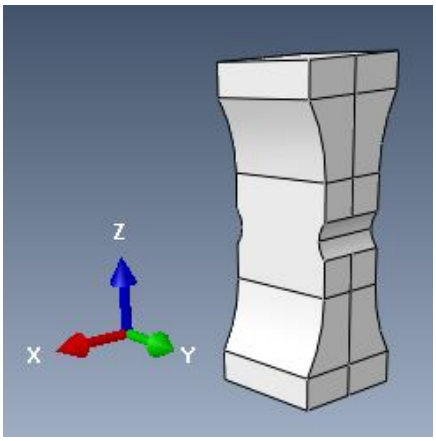

Figure 3.2: Geometry of the sample and reference system

3.3 Material properties

The orthotropic elastic material properties at the testing temperature have been inserted in Abaqus in the stiffness form according to [18]. These equations require only three independent elastic constants: Young's modulus (E), shear modulus (G) and Poisson ratio (ν). The coefficients of the stiffness matrix are inserted as if the crystal was oriented parallel to the [001] orientation. This is the reason why crystallographic orientation must be inserted afterwards. The material properties at temperature can be found in Table 3.2.

Material	CMSX-4
Temperature	550°C
E (GPa)	110
G (GPa)	114
ν (-)	0.39

Table 3.2: Material properties at temperature [6]

3.4 Crystallographic orientation and reference systems

Defining the crystallographic orientation in Abaqus is a key step in the analysis of anisotropic materials. To do that, it is required to know the crystallographic angles and how are they defined with respect to a reference. Rolls-Royce uses a criterion in which six characteristic angles fully define the position of the crystal in the space: θ, κ, α, ρ, γ and δ.

After analysing the role of each angle[2], it has been found that the position of the crystal, and therefore the local coordinate system (i.e. the material coordinate system), can be defined by using only three angles: γ, δ and κ[3], which are three consecutive rotations around <001> axes. According to Rolls-Royce criteria, γ is a rotation around the Y_0 axis, δ is a rotation around the X_1 axis and κ is a rotation around the Z_2 axis. These rotations are mathematically represented in Equation 3.1.

$$R_x(\delta) = \begin{pmatrix} 1 & 0 & 0 \\ 0 & \cos(\delta) & \sin(\delta) \\ 0 & -\sin(\delta) & \cos(\delta) \end{pmatrix} \qquad R_y(\gamma) = \begin{pmatrix} \cos(\gamma) & 0 & -\sin(\gamma) \\ 0 & 1 & 0 \\ \sin(\gamma) & 0 & \cos(\gamma) \end{pmatrix}$$

$$R_z(\kappa) = \begin{pmatrix} \cos(\kappa) & \sin(\kappa) & 0 \\ -\sin(\kappa) & \cos(\kappa) & 0 \\ 0 & 0 & 1 \end{pmatrix} \tag{3.1}$$

[2]The value of these angles for the specimens used will be omitted from the analysis due to confidentiality issues.

[3]κ is a clockwise rotation around one of the <001> axis. Therefore it must be inserted negatively in the equations.

By using these consecutive rotations, it is possible to calculate the matrix which links the global coordinate system with the local (i.e. material) one by applying Equation 3.2. Thus, any vector in the global coordinate system can be transformed to the local.

$$R_{Global->Local} = R_z(\kappa) \cdot R_x(\delta) \cdot R_y(\gamma) \tag{3.2}$$

Likewise, by using the inverse of these matrices, it is possible to convert a vector given in the local coordinate system to the global one (Equation 3.3). Thereby, it is possible to calculate the coordinates of the unit vectors which determine the axes of the local coordinate system measured in the global coordinate system (Cartersian notation). As an example, the position of the local axes measured in the global coordinate system can be determined by using Equation 3.4. This procedure is used to define the crystallographic orientation in Abaqus.

$$R_{Local->Global} = R_y^{-1}(\gamma) \cdot R_x^{-1}(\delta) \cdot R_z^{-1}(\kappa) \tag{3.3}$$

$$\begin{aligned}
\overrightarrow{X}_{Global} &= R_{Local->Global} \cdot \overrightarrow{X}_{Local} = R_{Local->Global} \cdot (1, 0, 0) \\
\overrightarrow{Y}_{Global} &= R_{Local->Global} \cdot \overrightarrow{Y}_{Local} = R_{Local->Global} \cdot (0, 1, 0) \\
\overrightarrow{Z}_{Global} &= R_{Local->Global} \cdot \overrightarrow{Z}_{Local} = R_{Local->Global} \cdot (0, 0, 1)
\end{aligned} \tag{3.4}$$

Figure 3.3[4] shows the equivalence between the two different reference systems used in this work: i) Cartesian coordinate system defined automatically by Abaqus (X-Y-Z) and ii) Miller coordinate system used in the definition of the slip systems ([100]-[010]-[001]). The fact of making coincident the components of both reference systems will be advantageous in the procedure described in Section 3.7, as the normal of the slip planes given in Table 2.1 in the Miller system can be used as the local Cartesian coordinates of the crystal. Additionally, Figure 3.3 shows the tensorial notation which will be employed

[4] See also Figure 3.2 to associate the reference systems used to the sample.

in Section 3.6.

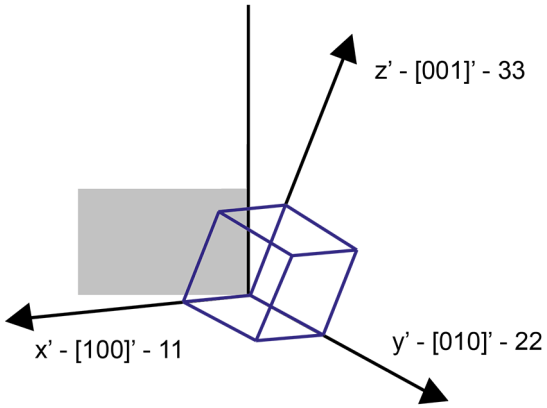

Figure 3.3: Reference systems definition in an arbitrarily rotated crystal: Cartesian, Miller and tensorial

The fact of defining the crystallographic orientation in Abaqus has an advantage with respect to rotate the stiffness matrix and insert these coefficients in the software. By doing this, Abaqus outputs the stress and strain components in the local coordiante system [18]. As mentioned in Section 3.6, obtaining the stress components in the local coordinate system will accelerate the post-processing of the data.

3.5 Load and boundary conditions

The load and boundary conditions have been imposed as in the experimental test (see Figure 3.4). The load condition is the one that reaches 419 MPa at the minimum section location, which is the base of the notch. Thus, the measures of the simulated sample makes the applied pressure to be 366.625 MPa.

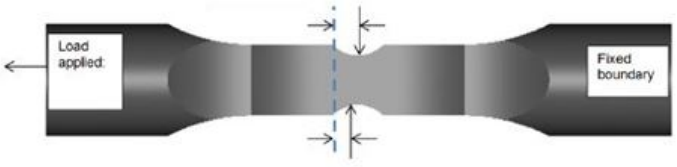

Figure 3.4: Load and boundary conditions. Source: Rolls-Royce

3.6 Stress projection into slip systems

This section explains the mathematical procedure to project the global stress into the slip systems. The slip systems are described in Table 2.1 and represented in Figure 3.5[5]. The process is based on the Schmid's Law (see Equation 2.3) and consists in quantifying the shear stresses resolved on the slip planes. As explained in Chapter 2, Schmid's Law make use of the stress tensor (σ), the angle between the applied load and the slip direction (λ) and the angle between the applied load and the normal to the slip plane (ϕ). The former one depends on the case study and it has to be extracted from Abaqus. The latter ones are geometrical angles that remain constant if the stress tensor is output in the material (i.e. local) coordinate system. In this scenario, the analysis can be done as if the crystal was parallel to the [001] direction and λ and ϕ can be easily calculated with Equation 3.5.

For a FCC crystal loaded in a [001] direction, ϕ is the angle between the normal to the (111) slip plane (i.e. the [111] direction) and the [001] direction. Using Equation 3.5 with $u = (1,1,1)$ and $v = (0,0,1)$, it can be obtained the value of $\phi = 54.7°$. Likewise, λ represents the angle between the slip direction ([110]) and the loading direction ([001]). Using Equation 3.5 with $u = (1,1,0)$ and $v = (0,0,1)$, the obtained value is $\lambda = 45°$.

$$\beta = \cos^{-1}\left(\frac{u_1v_1 + u_2v_2 + u_3v_3}{\sqrt{(u_1^2 + u_2^2 + u_3^2)(v_1^2 + v_2^2 + v_3^2)}}\right) \tag{3.5}$$

Equation 3.6[6] shows the expansion of the Schmid's Law under these conditions to the 12 slip systems [1]. It will be used to quantify the resolved shear stresses on the slip systems. The only condition to use this formula is that the stress tensor must be given in the material coordinate system. For further understanding see Figure 3.3 where the relationship between the tensorial notation and the Miller notation is given and Figure 3.5 where the direction of each slip system is depicted.

[5] To be consistent with the work presented until now, the slip systems are represented under the reference system used in this project.

[6] Note: $\cos(\lambda)\cdot\cos(\phi) = \cos(45)\cdot\cos(54.7) = \frac{1}{\sqrt{6}}$. The Equation is highly dependent on the reference system used.

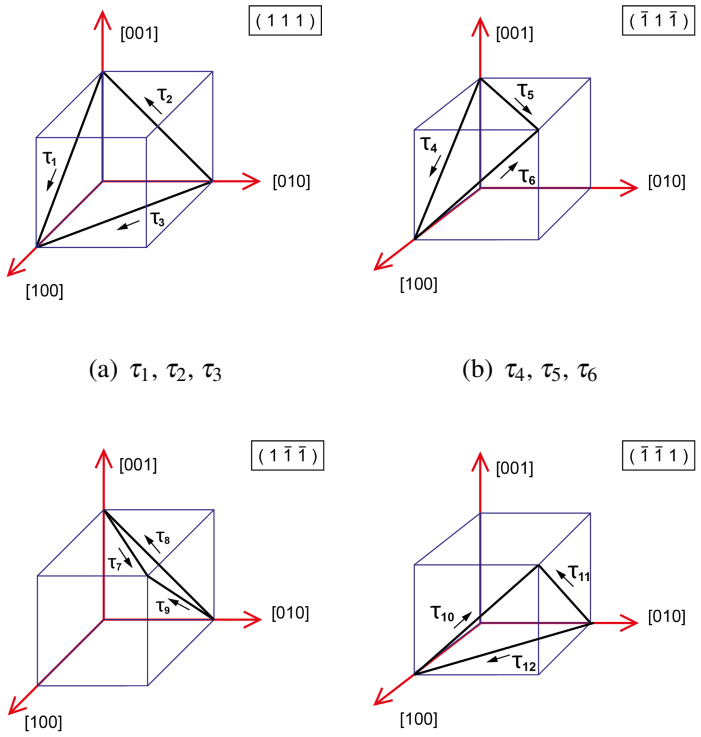

(a) τ_1, τ_2, τ_3 (b) τ_4, τ_5, τ_6

(c) τ_7, τ_8, τ_9 (d) τ_{10}, τ_{11}, τ_{12}

Figure 3.5: FCC slip systems

$$\begin{pmatrix} \tau_1 \\ \tau_2 \\ \tau_3 \\ \tau_4 \\ \tau_5 \\ \tau_6 \\ \tau_7 \\ \tau_8 \\ \tau_9 \\ \tau_{10} \\ \tau_{11} \\ \tau_{12} \end{pmatrix} = \frac{1}{\sqrt{6}} \begin{pmatrix} -1 & -1 & 0 & 0 & 1 & 1 \\ 0 & 1 & -1 & 1 & 0 & -1 \\ -1 & 0 & -1 & 1 & 1 & 0 \\ 1 & -1 & 0 & 0 & 1 & -1 \\ 1 & 0 & 1 & -1 & 1 & 0 \\ 0 & 1 & 1 & -1 & 0 & 1 \\ -1 & 0 & 1 & 1 & 1 & 0 \\ 0 & 1 & -1 & -1 & 0 & 1 \\ -1 & 1 & 0 & 0 & 1 & 1 \\ 0 & 1 & 1 & 1 & 0 & -1 \\ 1 & 1 & 0 & 0 & 1 & -1 \\ 1 & 0 & -1 & -1 & 1 & 0 \end{pmatrix} \cdot \begin{pmatrix} \sigma_{11} \\ \sigma_{12} \\ \sigma_{13} \\ \sigma_{22} \\ \sigma_{23} \\ \sigma_{33} \end{pmatrix} \tag{3.6}$$

The RSS will be used to plot them as a field along the crack path and determine which ones are dominating. Similarly, RSS will be used to compute the Q factors (see Chapter 2) and plot them as a field along the crack path. This graph is expected to detect single slip and multislip regions along the crack path.

3.7 Slip plane trace estimation

This section explains the procedure to calculate the direction of the dominant slip plane in the single slip regions. The first step consists in rotating the normal of the slip plane from the local to the global coordinate system by using the rotation matrix defined in Equation 3.3 as shown in Equation 3.7. These normals are gathered in Table 2.1 in the Miller notation, which has been made coincident to the Cartesian coordinate system ($\overrightarrow{n}_{Local}$). Therefore, Miller notation can be used as the local Cartesian coordinate system. Afterwards, the normal of the slip planes in the global coordinate system must be projected into the surface (i.e. make the thickness component (X direction) 0) and rotate it 90° to make it parallel to the slip plane trace on the surface. Finally, it is immediate to calculate the angle of the slip trace with respect to a reference, which in this case will be the Y axis simulating the normal orientation, by using Equation 3.5.

$$\overrightarrow{n}_{Global} = R_{Local->Global} \cdot \overrightarrow{n}_{Local} \tag{3.7}$$

The crack path in the single slip regions should take the direction of the dominant slip plane, which can be easily calculated following the steps described above.

3.8 FEA Models

Two different anisotropic elastic models have been developed to understand the crack path in notched single crystals: i) model without growing the crack and ii) model growing the crack. The main difference between them are:

- The model growing the crack incorporates the stress intensification provided by the crack tip
- The model growing the crack incorporates the influence of the cross-sectional area reduction
- The model growing the crack incorporates the rotation that the specimen suffers as it is being deformed
- Neither of the models incorporate plasticity effects

The only aspect that can be addressed in the model without growing the crack is the area reduction effects. These effects can be considered in the simplified analysis without growing the crack by multiplying Equation 3.6 by a correction factor (CF). CF can be obtained by defining the stress that the remaining cross-section would have to withstand (Equation 3.9).

$$A_{new} = A_0 - b \cdot t \tag{3.8}$$

$$\sigma_{new} = \frac{A_0}{A_{new}} \cdot \sigma_{applied} = CF \cdot \sigma_{applied} \tag{3.9}$$

where A_0 is the initial cross-sectional area, b is the crack length and t is the thickness of the specimen.

3.8.1 Anisotropic elastic model without growing the crack

This model computes the stress tensor along the whole crack path without growing the crack. Therefore, is a very simplistic model that will be used as a first approach to the problem. The feasibility of this model will be analysed by comparing the results obtained with the model growing the crack. A priori, the error generated with this model will increase with the length of the crack due to the absence of rotation of the sample as the crack advances.

3.8.2 Anisotropic elastic model growing the crack

This model is represented in Figure 3.6 for Specimen A. The reason for developing this model is to include some of the effects that are not considered in the simplified model and use it to validate the results obtained with the model without growing the crack. The sequence of pictures in Figure 3.6 shows the deformed shape with the crack having grown until the vicinity of each measurement point. The process itself is more time consuming and the computational capacity required is slightly higher. The stress tensor is captured only in the measurements points (notch, P1, P2, P3 and P4 in Figure 3.6). This model has been developed only for Specimen B.

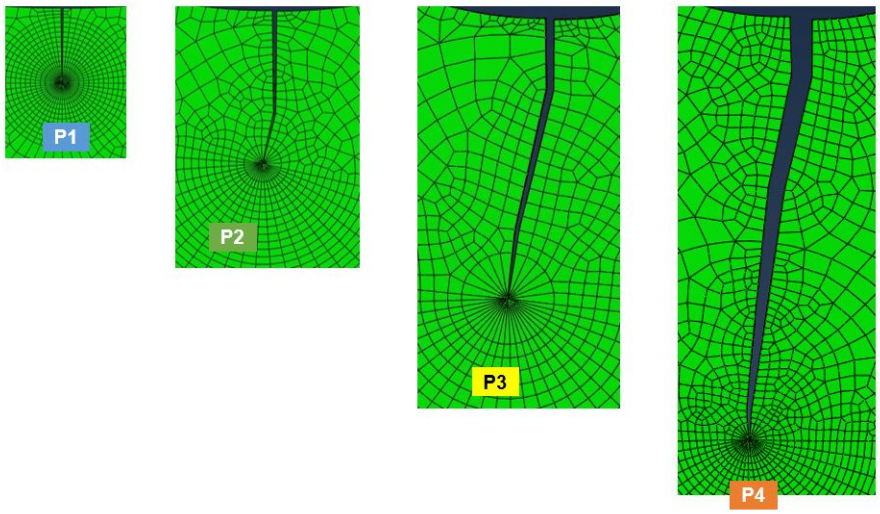

Figure 3.6: Crack path modelling for Specimen B (deformed view)

Chapter 4

Results

4.1 Introduction

This chapter aims to present the results obtained with the FE models developed to analyse the crack path in notched single crystals. The results will be mostly provided in the form of graphs. The two main graphs that are going to be used will be termed the RSS graph and the Q graph. RSS graph[1] provides information about the evolution of the absolute value of the shear stresses resolved on the slip systems ($|\text{RSS}|$) along the crack path versus the distance from the notch measured along the Y axis (perpendicular to the applied load). Similarly, the Q graph plots the evolution of the Q factor along the crack path against the distance from the notch measured along the Y axis.

RSS graph incorporates the $CRSS = 376$ MPa with a $\pm 15\%$ band error superimposed on it (dashed lines in Figures 4.2 a), 4.3 a) and 4.4 a)). This band error must be applied since the heat treatment and the volume fraction of γ' are unknown for the material tested. Similarly, Q factor graph incorporates the range border between the single slip and multi-slip conditions as appears in the literature $Q = 0.9 - 0.93$ (dashed lines in Figures 4.2 b), 4.3 b) and 4.4 b)). Likewise, the vertical dotted lines depicted in all these Figures represents a change in crack path direction (i.e. these lines are located in the yellow circles of

[1] This graph plots only the highest 6 slip systems in magnitude.

Figure 4.1).

RSS graph reveals information about the dominant slip system in each region of the crack path. Besides, it gives information about the activation or deactivation of the slip systems (i.e. if they are above or below the CRSS). Q graph might be used to distinguish single slip from multislip regions within the crack path. The combination of the information provided by both graphs will be used to determine the changes in crack path direction and the slip condition. In the case of finding a single slip condition, which would be defined by $Q < 0.9$ and only one slip system with $RSS > CRSS$, the angle that the dominant slip plane forms with the plane perpendicular to the applied load would be computed. This angle would be compared to the one measured in the fractography images (Figure 4.1). The difference between both figures will determine if this procedure can be used to predict the crack path in single slip regions.

4.2 Fractography

The fractography of the failed samples is used to define the crack path in Abaqus and to compare the trace of the dominant slip plane on the surface with the crack direction in the single slip regions. All the specimens have the same cross-sectional area and were tested under the same conditions. The only difference between them is the crystallographic orientation. Figure 4.1 shows the crack path of the specimens under examination. The yellow circles highlight the changes in crack path direction. The analysis will be done until the last yellow point in each specimen. The rest is considered fracture zone. The images in Figure 4.1 correspond to the middle thickness (i.e. the pictures were taken after cutting the sample through the middle). The stress tensor in the FE simulations will be captured at the same location.

As it can be seen in Figure 4.1, the crack in Specimen A does not start at the minimum area location. The initiation point is upwards the middle of the notch, indicating that the crack started in an inclusion or surface irregularity. The same trend is found in Specimen

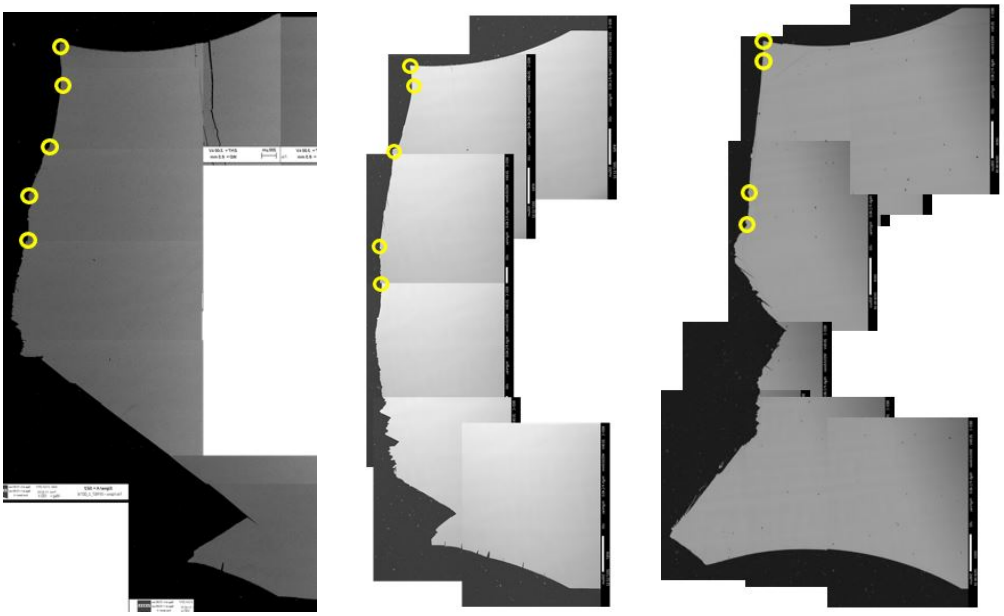

(a) Specimen A (b) Specimen B (c) Specimen C

Figure 4.1: Fractography images of the analysed specimens

C. By contrast, Specimen B has the initiation point in the middle of the notch, indicating that the crack has started here due to the notch intensification and is supposed to be surface defect free. The propagation of the crack follows similar trends in all the specimens, growing initially in the plane perpendicular to the loading direction (or very close to it) and suddenly transitioning towards a slanted orientation. Finally, the crack comes back to the normal orientation until it flows into the fracture zone, which is out of the scope[2] in this project.

4.3 Model without growing the crack

4.3.1 Specimen A

Results for Specimen A are shown in Figure 4.2. According to the RSS graph, there is not a clear dominant slip system along the crack path. Only in the vicinity of the notch the contribution of τ_2 and τ_{11} are more significant than the remaining slip systems. Namely,

[2]The greatest percentage of fatigue life occurs in the zone that it is being analysed. The life spent in the fracture zone is negligible in comparison. This is the reason why it is out of the scope.

τ_2 dominates in the region close to the notch, until the first change in crack path direction, when τ_6 becomes equally dominant. The incorporation of τ_6 to the propagation of the crack explains the change in crack path. Likewise, the second transition can be explained by the simultaneous incorporation of several slip systems (e.g. τ_1, τ_9, τ_{11}) to crack growth behaviour, as seen in Figure 4.2 a).

Q factor graph reveals that the whole crack path is growing under multislip conditions. Therefore, it would not be possible to predict the crack path for this specimen.

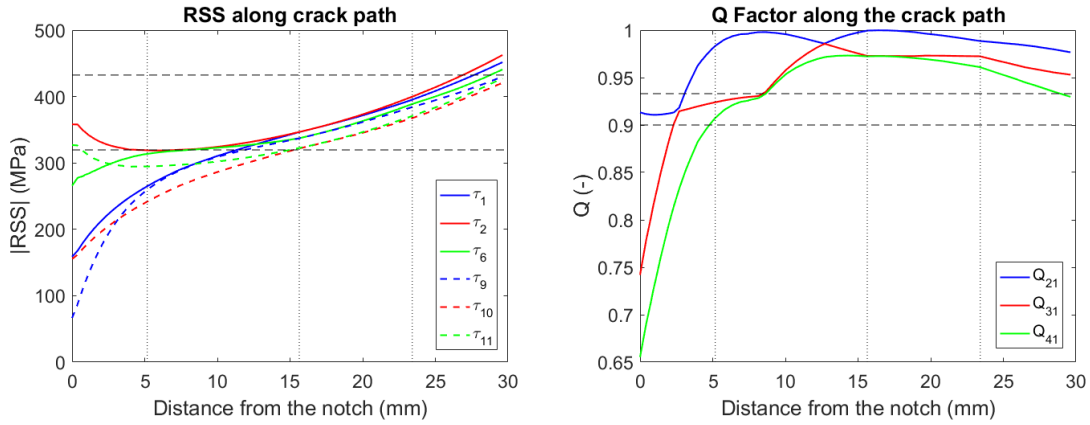

(a) RSS (MPa) (b) Q Factor (-)

Figure 4.2: Model without growing the crack: Specimen A

4.3.2 Specimen B

Results for Specimen B are shown in Figure 4.3. According to the RSS graph, there is a clear dominant slip system along the crack path (τ_{10}). This slip system controls the crack propagation. The second dominant slip system is τ_8, which leads in the first region but as the distance from the notch is increased it loses dominance in favour of τ_{10}. The departure from the normal direction is produced when τ_{10} overcomes τ_8 and begins to dominate.

Q graph seems to reveal a well-differentiated single slip region along a great part of the crack, with $Q < 0.933$ from the first transition. However, τ_8 remains above the CRSS, so it must be considered active and participating in crack growth even though $Q < 0.9$. Towards the end of the graph, Q factor increases and reaches $Q = 0.9$ (i.e.

multislip conditions) in the last transition, which could explain why the crack goes back to the normal orientation due to the increasing influence of the secondary slip system (τ_8). Besides, the shear stress resolved on several slip systems (e.g. τ_1, τ_4, τ_{11}) increases with the distance from the notch and eventually overcomes the CRSS, which may explain their influence in the crack growth behaviour and the change in direction.

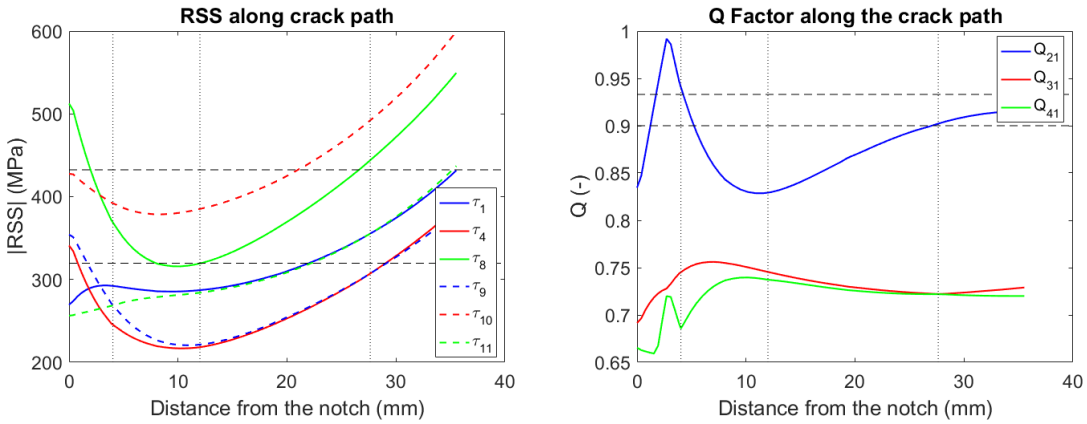

(a) RSS (MPa) (b) Q Factor (-)

Figure 4.3: Model without growing the crack: Specimen B

4.3.3 Specimen C

Results for Specimen C are shown in Figure 4.4. The trend is similar to the on of Specimen A. According to the RSS graph, there is not a clear dominant slip system along the crack path. Only in the vicinity of the notch the contribution of τ_4 and τ_{11} are more significant than the remaining slip systems. The departure from the normal orientation occurs when τ_4 and τ_{11} lose dominance in favour of τ_8 and τ_{10}.

Q factor graph reveals that the whole crack path is growing under multislip conditions, with τ_8 and τ_{10} contributing mostly to crack growth behaviour. Therefore, it would not be possible to predict the crack path for this specimen.

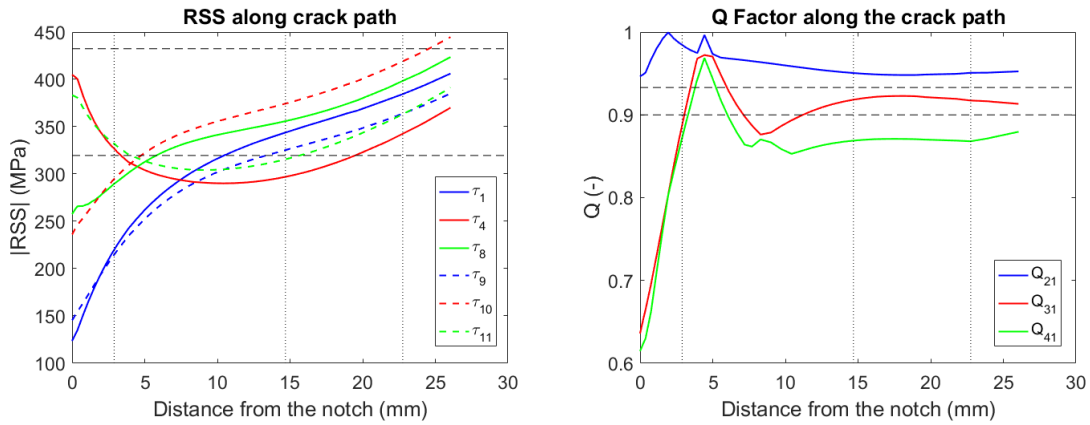

(a) RSS (MPa) (b) Q Factor (-)

Figure 4.4: Model without growing the crack: Specimen C

4.4 Model growing the crack

The results of the model growing the crack are presented in Figure 4.5 for Specimen B. The stress tensor was only captured in 5 points along the crack path. By comparing Figures 4.3 and 4.5, it can be seen that both models follow the same trend, with τ_{10} being the dominant slip system along the greatest part of the crack path. Nevertheless, the contribution of the second and third dominant slip systems varies significantly between the two models. This modification may be explained by the change in the stress field near the measurement points, which in this model is significantly controlled by the sharp crack tip. This modified stress field is strengthening the participation of some slip systems (e.g. τ_{10}) and reducing the one of others (e.g. τ_8).

4.5 Slip Traces

The procedure described in Section 3.7 explains how to calculate the trace of the slip planes in the surface. The trace of the dominant slip plane in the single slip regions should match the crack path direction since in this conditions there is only one slip system contributing to crack growth, thus the crack should grow along this preferential plane. In the multislip regions, the crack path direction should be a weighted average of all the traces

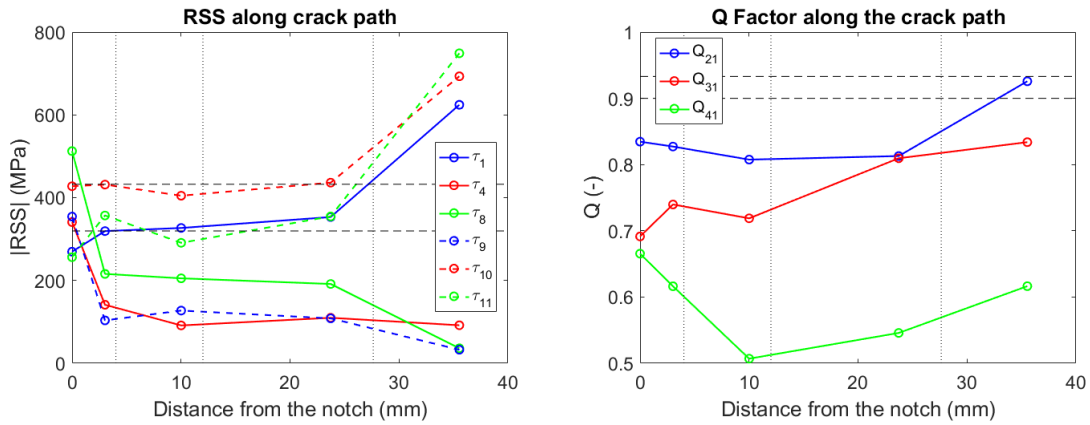

(a) RSS (MPa) (b) Q Factor (-)

Figure 4.5: Model growing the crack: Specimen B

of the slip systems which are contributing to crack growth. How to create this weighted average is out of the scope because multislip condition implies the interaction of dislocations which has been emitted through different planes and this effect is difficult to model. Figure 4.6 depicts the crack direction measurements (from the plane perpendicular to the applied load). Table 4.1 represents the traces of the slip planes for the three specimens. A priori, anyone of these values should match the experimental ones since no single slip region has been detected. As a consequence, more specimens should be tested until find a well-defined single slip region in which the procedure explained in Section 3.7 can be validated.

Slip systems	Specimen A	Specimen B	Specimen C
τ_1, τ_2, τ_3	$6.8°$	$-15.4°$	$-34.7°$
τ_4, τ_5, τ_6	$56.7°$	$43.1°$	$46.3°$
τ_7, τ_8, τ_9	$-52.7°$	$-67.3°$	$-54.4°$
τ_{10}, τ_{11}, τ_{12}	$-2.0°$	$-4.9°$	$41.2°$

Table 4.1: Predicted slip plane traces on the surface for different specimens

Although a priori it was out of the scope, the author has decided to include in Figure 4.6 the crack path direction in the fracture zone. This has been made to highlight the similarities between the predicted slip traces in Table 4.1 and the path undergone by the cracks in this region. It is important to mention that more samples have been analysed

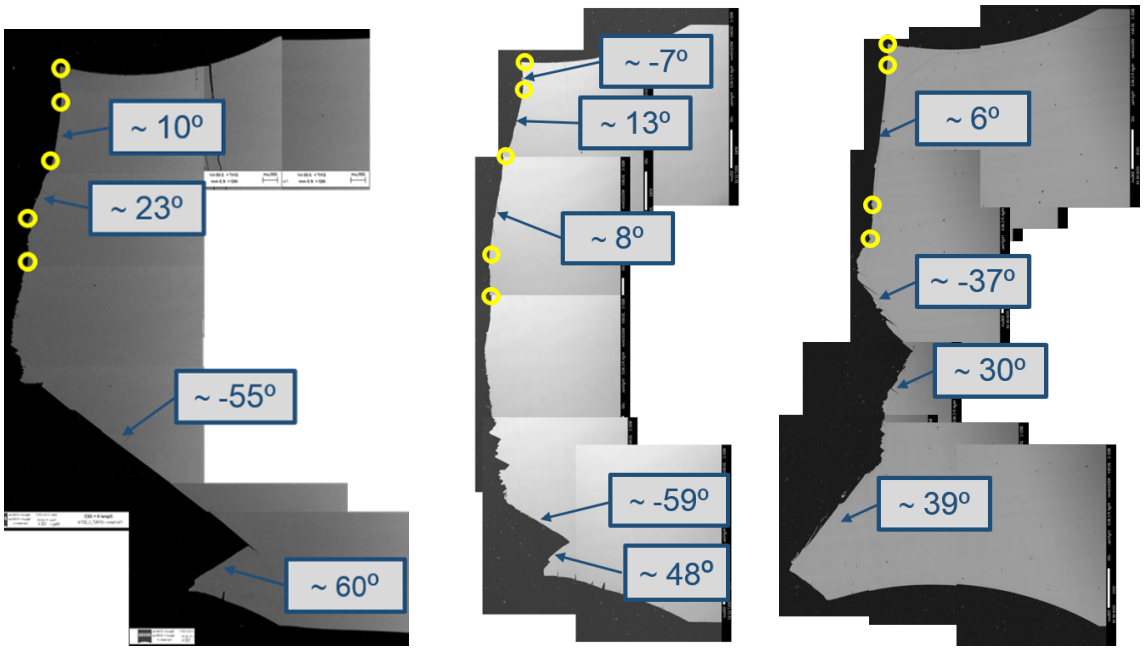

(a) Specimen A (b) Specimen B (c) Specimen C

Figure 4.6: Experimental crack path directions

apart from the ones presented in this document, and the same similarity has been found between the predicted and the experimental crack path directions in the fracture zone. A possible reason for this will be presented in Chapter 5.

Chapter 5

Discussion

Results presented in Chapter 4 demonstrate that the change in crack path direction is driven by the activation/deactivation of a specific number of slip systems and might be explained by the simultaneous analysis of RSS and Q factor graphs. However, the direction of the crack after it deviates from the former orientation cannot be matched with the analysis done in Sections 3.7 and 4.5 because it was not possible to find a well-defined single slip condition. This chapter aims to discuss about the validity of the results with the objective of assessing the aspects that may be influencing them. The main topics described in here will be: model simplifications, microstructure interaction and corrosive environment.

As explained in Section 3.8, the model without growing the crack is a very simplistic model that lacks the rotation of the sample while it is being deformed and the plasticity and stress concentration effects at the crack tip. However, it has been demonstrated that it can predict the crack direction changes quite accurately. The fact of disregarding the rotation of the crack introduces error in the procedure described in Section 3.7. The sample, and consequently the crystal, becomes slightly rotated during the loading cycles due to the bending moment caused by the asymmetry of the cross-section and the applied load. Hence, the position of the slip systems varies with respect to the initial position, and the contribution to crack growth behaviour varies as well. As a result, the crack path

measurements in Figure 4.6 would never exactly match the results in Table 4.1. Likewise, the error introduced in the model without growing the crack increases with the length of the crack due to the absence of cracking, so the results obtained towards the end of the path must be studied with consideration. In addition, the fact of ignoring plasticity effects as well as the stress concentration produced at the crack tip generates error in the RSS magnitude, with the calculated values being probably lower that the actual ones.

After incorporating the cracking it has been found that the two models follow the same pattern regarding the dominant slip system but a different one concerning the second and third dominant slip systems. This can be explained due to the change in the stress field ahead of the crack tip due to the stress intensification. In this way, the most reliable model would be the model growing the crack. However, neither of those models incorporates plasticity. As a consequence, the stress field is not accurately represented in neither of the models because of the absence of plasticity criteria in the analysis, which would introduce the non-linearity effects characteristic of the yield condition.

The interaction of the crack with the microstructure is another aspect that may be influencing the results. As γ' precipitates are much stronger than the matrix γ, the shear stress required to cut a γ' precipitate is considerably higher than the shear stress required to move a dislocation though the matrix. In regions where the driving force is locally decreased, the slip can be confined to only the matrix, generating an effect which would make the crack to grow under non-crystallographic planes perpendicular to the loading axis. This is the main feature of the opening mode fatigue failure. Therefore, for crack lengths small compared to the width of the sample, the fatigue failure would be dominated by the opening mode, indicating that shear stresses are not fully controlling crack propagation. By contrast, once the crack has reached certain size, the stress concentration at the crack tip together with the inability of the remaining cross-section to withstand the applied stress will increase the driving force. Hence, it would be easier to cut a γ' precipitate and the failure mode would be purely shearing. A caveat to this is that this fracture zone is associated with an unstable catastrophic phenomenon, and the work performed

here has not reach that levels of complexity. Regardless of that, it is important to mention that in these unstable failure regions, all the samples studied in here (see Figure 4.6) match, with a degree of error of around $\pm 7^{\circ}$, any of the predicted slip traces in Table 4.1, which may indicate a purely shearing failure mode under single slip conditions. Further work remains to be done in this area to corroborate this hypothesis since the analysis done here gathers only the propagation stage and not the fracture zone.

Furthermore, the influence of the corrosive environment created in the testing chamber has been omitted of this analysis. However, as the crack path changes can be justified without taking these effects into account, it can be concluded that the corrosion effects do not play an important role in the propagation of the crack, although they may be having a significant influence in the incubation and initiation stages. Despite this, a much deeper analysis remain to be done regarding the effect of the corrosion products in the crack behaviour.

Ultimately, it is important to mention that the whole process involves several inherent errors, such as the technique for measurement of the crystallographic angles, the crack path modelling in Abaqus or the discretization error of the FEA. The influence of these types of errors in the results is expected to be not relevant.

Chapter 6

Conclusions

The main conclusions of the project are:

- Crystallographic orientation plays a significant role in the activation of slip systems and therefore in the crack propagation mechanism. Different crystal orientations entail different crack paths.
- Crack growth behaviour in single crystal nickel based superalloys is governed by dislocation-based shearing processes.
- Shear stresses resolved on the slip systems are controlling plastic deformation and consequently crack growth. The mathematical tool to quantify those is the Schmid's Law.
- CRSS is a key property to understand crack growth behaviour in single crystals. However, it varies with temperature, heat treatment, volume fraction of γ' and cyclic deformation, so it is a difficult material property to deal with.
- The simultaneous analysis of RSS and Q graphs along the crack path reveals the crack deviations. RSS graph is used to estimate how many slip systems are activated. Q graph is used to confirm the slip condition along the crack path.

- Crack deviations can be explained as: i) sudden incorporation/reduction of the number of slip systems contributing to crack growth (i.e. activation/inhibition of slip systems), ii) among the activated slip systems, a change in the dominant one.

- No specimen was found with a clear single slip condition. Therefore, the procedure explained here to predict the crack path in those regions has not been validated. Run the test under the high cycle fatigue (HCF) regime would help to find a single slip condition.

- As the crack paths deviations can be explained using only mechanical related concepts, it can be concluded that the crack path direction is driven by mechanical propagation. Nevertheless, it would be worthy to find a specimen with a well-defined single slip condition and study whether the crack path can be predicted in this region or not.

Overall, this project has intended to gain knowledge in the fatigue failure mechanism of turbine blades by studying the crack behaviour in notched single crystals. Particularly, the work described in here has been focused on understanding the changes in crack path direction. The procedure developed to approach the solution has demonstrated that these changes respond to the fluctuation of the shear stresses resolved on the slip planes along the crack path. In addition, the procedure to predict the crack path direction in the single slip regions has been presented, but it has not been validated due to the lack of single slip conditions along the crack paths.

Chapter 7

Future Work and Recommendations

This chapter proposes several topics to cover in the future in order to acquire a complete knowledge of the fatigue crack propagation mechanisms in notched single crystals and, eventually, in turbine blades.

A very interesting aspect to address would be the estimation of the crack growth rate in each region and confirm the findings in [17], which postulates that a crack growing in single slip condition grows slower than a crack growing under multislip conditions. If this can be verified, blade designers might focus on finding the crystallographic orientation that maximises single slip regions under the loading condition in service. The recommended procedure consists in finding the crystal position that makes the second dominant slip system to remain below the cyclic critical resolved shear stress for a prolonged period. To achieve that, it is recommended to run the experiments under the high cycle fatigue regime (i.e. with a lower applied load). This would increase the fatigue life of the blades without increasing the cost nor the weight.

Furthermore, extrapolating the fractography analysis to 3D would help to locate the $\{111\}$ planes physically on the failed surface. This information would enhance and clarify the 2D analysis made in Section 3.7.

Additionally, it would be advantageous to repeat the testing under a corrosion-free environment and post-process the results as indicated in this work. This would ensure

that the fatigue crack propagation stage is driven by mechanics. Similarly, repeating the testing under vacuum would produce a set of results which can be used to compare them with the ones tested under a chemically active environment. The difference between them would highlight the effects of corrosion products in crack propagation.

Likewise, develop a crystal plasticity model to assess the impact of plasticity in crack propagation would be beneficial for the complete understanding of fatigue degradation mechanisms in single crystals. This analysis is expected to be more computationally demanding than the ones developed in this project but would account for the non-linearity effects of the stress state during the deformation of the crystal. It would be advantageous to include in this model a routine in which the elements intersecting the crack path are subsequently removed in each step, simulating the crack growth, and the stress tensor is captured in each of those steps. This would be the optimum FE model to understand the fatigue failure mechanism.

Ultimately, all the knowledge collected throughout this study as well as the outcomes of the points presented above should be extrapolated to real blades with their correspondent geometry and boundary conditions. This would be the scenario that blades will face in service and therefore will be the next logical challenge to address.

References

[1] N. K. Arakere and G. Swanson. Effect of Crystal Orientation on Fatigue Failure of Single Crystal Nickel Base Turbine Blade Superalloys. *Journal of Engineering for Gas Turbines and Power*, 124(1):161, 2002.

[2] William D Callister. *Materials Science and Engineering: An Introduction*. 7th edition, 2007.

[3] W. Qiu, X. Ma, S. Rui, and H.-J. Shi. Crystallographic analysis on small fatigue crack propagation behaviour of a nickel-based single crystal superalloy. *Fatigue & Fracture of Engineering Materials & Structures*, 40(1):3–11, 2017.

[4] N K Arakere, S Siddiqui, and F Ebrahimi. Evolution of plasticity in notched Ni-base superalloy single crystals. *International Journal of Solids and Structures*, 46(16):3027–3044, 2009.

[5] K. Tanaka, T. Hoshide, and N. Sakai. Mechanics of fatigue crack propagation by crack-tip plastic blunting. *Engineering Fracture Mechanics*, 19(5):805–825, 1984.

[6] A. Sengupta, S. K. Putatunda, L. Bartosiewicz, J. Hangas, P. J. Nailos, M. Peputapeck, and F. E. Alberts. Tensile behavior of a new single-crystal nickel-based superalloy (CMSX-4) at room and elevated temperatures. *Journal of Materials Engineering and Performance*, 3(1):73–81, 1994.

[7] Koji Kakehi. Influence of Primary and Secondary Crystallographic Orientations

on Strengths of Nickel-based Superalloy Single Crystals. *Materials Transactions*, 45(6):1824–1828, 2004.

[8] Ma X He Z, Qiu W, Fan YN, Han QN, Shi HJ. Effects of secondary orientation on fatigue crack initiation in a single crystal superalloy. *Fatigue Fract Eng Mater Struct.*, 136(September):935–948, 2018.

[9] Sammy Tin and Tresa M Pollock. Nickel-Based Superalloys for Blade Application: Production , Performance and Application. pages 1–14, 2010.

[10] Donald C. Stouffer and L.Thomas Dame. *Inelastic deformation of metals*. 1996.

[11] J. R. Rice. Limitations to the small scale yielding approximation for crack tip plasticity. *Journal of the Mechanics and Physics of Solids*, 22(1):17–26, 1974.

[12] P. Lukáš and L. Kunz. Small cracks - Nucleation, growth and implication to fatigue life. *International Journal of Fatigue*, 25(9-11):855–862, 2003.

[13] J Telesman and L J Ghosn. The Unusual Near-Treshold Fatigue Crack Growth Behaviour of a Single Crystal Superalloy and the Resolved Shear Stress as the Crack Driving Force. *Engineering Fracture Mechanics*, 34(5/6)(516):1183–1196, 1989.

[14] A Vattre. Strength of single crystal superalloys: from dislocation mechanisms to continuum micromechanics. *PhD thesis*, 2009.

[15] R. Pippan. Dislocation Emission and Fatigue Crack Growth Threshold. *Acta metall. mater.*, 39(3):255–262, 1991.

[16] Alex S. Cheng and Campbell Laird. Mechanisms of fatigue hardening in copper single crystals: The effects of strain amplitude and orientation. *Materials Science and Engineering*, 51(1):111–121, 1981.

[17] Jack Telesman and Peter Kantzos. Fatigue Crack Growth Behavior of a Single Crystal Alloy as Observed Through an In Situ Fatigue Loading Stage. *NASA Technical Memorandum*, SAMPE Meta, 1988.

[18] Dassault Systèmes Simulia. Abaqus 6.14 CAE User Guide. 2014.

Appendix A

Specimen Measures

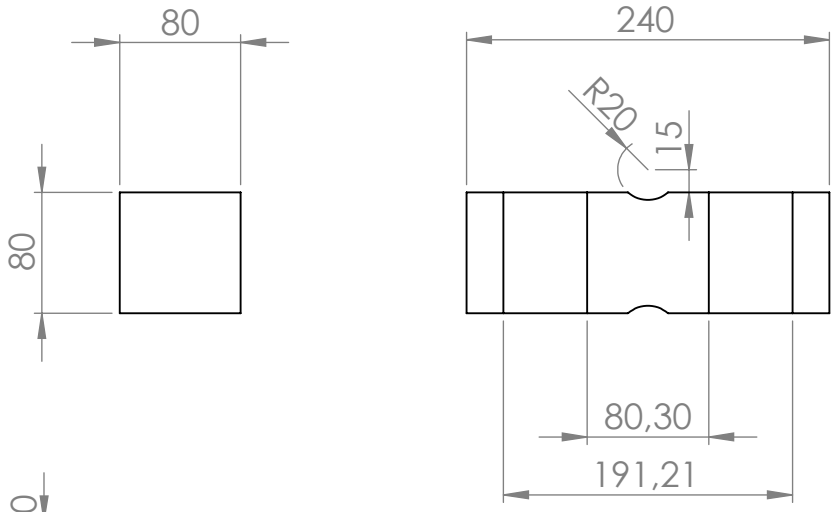

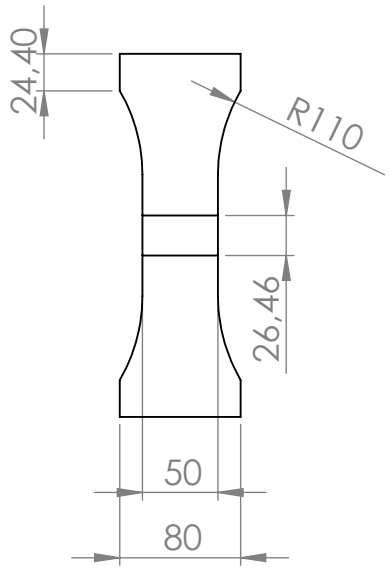

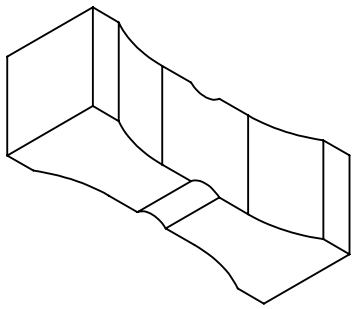

UNLESS OTHERWISE SPECIFED DIMENSIONS ARE IN MILIMETERS	**PROJECTION**				DO NOT SCALE DRAWING	**REV.**
#	**ADDITIONAL APPROVALS**	**DATE**				**PROJECT TITLE**
1	MATERIALS & PROCESSES					ASSESSMENT OF FATIGUE CRACK PATHS IN SINGLE CRYSTALS FROM TURBINE BLADES
2	QUALITY ASSURANCE					
3	MANUFACTURING					
4	TREATMENT					
			MATERIAL		**DRAWN TITLE**	A4
			CMSX-4		MODELLED SAMPLE MEASURES	
DATE	27/07/2018		**WEIGHT**		**SCALE** 1:5	**SHEET**

Appendix B

CURES Approval: CURES/5495/2018

CURES Submission: Approved

donotreply@infonetica.net

Fri 01/06/2018 13:35

To: López Canos, Samuel <S.Lopez@cranfield.ac.uk>;

Cc: Castelluccio, Gustavo <castellg@cranfield.ac.uk>;

Dear Samuel

Reference: CURES/5495/2018
Title: Assessment of Fatigue Crack Paths in Single Crystals from Turbine Blades

Thank you for your application to the Cranfield University Research Ethics System (CURES).

Your proposed research activity has been confirmed as Level 1 risk in terms of research ethics. You may now proceed with the research activities you have sought approval for.

Please remember that CURES occasionally conducts audits of projects. We may therefore contact you during or following execution of your fieldwork. Guidance on good practice is available on the research ethics intranet pages.

If you have any queries, please contact cures-support@cranfield.ac.uk

We wish you every success with your project.

Regards

CURES Team

May we remind you of the importance of addressing health and safety issues in your research. Templates and further guidance are available here.

Appendix C

Word Extension Permission

RE: MSc Thesis Word Count

Castelluccio, Gustavo

Mon 13/08/2018 20:38

To: López Canos, Samuel <S.Lopez@cranfield.ac.uk>;

Permission granted. You have performed very well and it is justified the petition.

Gustavo M. Castelluccio, PhD
Research Senior Lecturer in Manufacturing
School of Aerospace, Transport and Manufacturing
Cranfield University

Cranfield, Bedfordshire, MK43 0AL, UK, Building 30
+44 (0) 1234 750111 x 2092
https://www.researchgate.net/profile/Gustavo_Castelluccio
www.cranfield.ac.uk/people/dr-gustavo-m-castelluccio-16991655

From: López Canos, Samuel
Sent: 13 August 2018 20:23
To: Castelluccio, Gustavo <castellg@cranfield.ac.uk>
Subject: MSc Thesis Word Count

Dear Gustavo,

The aim of this email is to confirm the permission to extend the maximum word length permitted in the thesis until 10000 words.

Regards,
Samuel